Journal of Systems Engineering and Electronics
Vol. 31, No. 2, April 2020, pp.403 – 414

Observer-based multivariable fixed-time formation control of mobile robots

LI Yandong[1,*], ZHU Ling[2], and GUO Yuan[1]

1. College of Computer and Control Engineering, Qiqihar University, Qiqihar 161006, China;
2. School of Mechanical and Electronic Engineering, Qiqihar University, Qiqihar 161006, China

Abstract: This paper proposes a multivariable fixed-time leader-follower formation control method for a group of nonholonomic mobile robots, which has the ability to estimate multiple uncertainties. Firstly, based on the state space model of the leader-follower formation, a multivariable fixed-time formation kinematics controller is designed. Secondly, to overcome uncertainties existing in the nonholonomic mobile robot system, such as load change, friction, external disturbance, a multivariable fixed-time torque controller based on the fixed-time disturbance observer at the dynamic level is designed. The designed torque controller is cascaded with the formation controller and finally realizes accurate estimation of the uncertain part of the system, the follower tracking of reference velocity and the desired formation of the leader and the follower in a fixed-time. The fixed-time upper bound is completely determined by the controller parameters, which is independent of the initial state of the system. The multivariable fixed-time control theory and the Lyapunov method are adopted to ensure the system stability. Finally, the effectiveness of the proposed algorithm is verified by the experimental simulation.

Keywords: multivariable fixed-time control, formation control, uncertainty, fixed time observer, nonholonomic mobile robot.

DOI: 10.23919/JSEE.2020.000017

1. Introduction

In recent years, the leader-follower method is widely used in mobile robot formation control because of its simplicity, reliability, and scalability. The formation will converge asymptotically through the controller [1 – 4]. However, when mobile robots perform certain tasks in a limited time to achieve the desired formation, such as military, rescue, and transportation, the methods of [1 – 4] do not work well. In order to overcome this problem, finite-time formation control of mobile robot was proposed in [5 – 11]. However, the convergence time or setting time of finite-time control depends on the initial state. The initial state is generally difficult to obtain, which makes it difficult to give an accurate estimate of the convergence time in advance. Recently, Polyakov's fixed-time theory provides a solution to this problem [12]. Unlike the finite-time control method, the fixed-time control method can ensure that the bounded convergence time is independent of the initial state of the system [13]. In [14], the robust fixed-time consensus tracking was studied for mobile robot formation. In [15], the fixed-time formation control of multi-robot system was studied in the consensus control framework. Both methods of [14,15] are in the framework of distributed consensus control, which are similar to those in [16 – 19]. These methods decouple a multivariate system into a control problem with a single input channel, which is solved through the fixed-time framework of scalar systems. These methods cannot be applied to the multivariable fixed-time control of multi-mobile robots.

In real applications, due to various uncertainties affecting mobile robots, such as load change, friction, and external disturbance, the robot kinematics control with the "perfect speed tracking" assumption cannot meet the requirements of the formation control system [1,2]. Therefore, the dynamic model of the robot and the design of resisting multiple uncertain disturbances should be considered. The effectiveness to overcome the uncertainty is critical to the performance of the control system. An effective way is to design a disturbance observer to estimate the uncertain parts of the system. Similarly, if an accurate estimate of the uncertain part can be achieved within a limited time, the control performance of the system will be improved. In [9 – 11], a finite-time observer was designed to estimate the uncertainty disturbance. However, similar to the finite-time controller, the observation time is affected by the initial state, which is difficult to obtain. In [20], a differentiator based on the fixed-time theory provided a solution to the similar problems, which was extended to multivariate situations in [21]. Inspired by [21], the multivariable

Manuscript received May 24, 2019.
*Corresponding author.
This work was supported by the National Natural Science Foundation of China (61872204) and the Natural Science Foundation of Heilongjiang Province of China (F2015025).

fixed-time observer is employed in this paper.

The contribution of this paper is threefold. First, the leader-follower multivariable fixed-time formation control with the uncertain multivariable fixed-time observer is proposed for the nonholonomic mobile robot system. Second, in any initial state, the effects of multiple uncertainties on the robot system is overcome in a fixed time. Third, the cascade multivariable fixed-time control of the nonholonomic mobile robot is presented, which provides a basic framework for the extended research of this kind of problem.

This paper is organized as follows. Section 2 presents models for the nonholonomic mobile robot and the kinematics of the leader-follower formation. The formation controller is designed in Section 3. The simulation and analysis of the proposed algorithm are presented in Section 4. Finally, Section 5 concludes this study.

2. Modeling

2.1 Model of nonholonomic mobile robot

The mathematical model of nonholonomic mobile robots is shown as follows [1–4]:

$$\dot{\boldsymbol{q}} = \begin{bmatrix} \dot{x} \\ \dot{y} \\ \dot{\theta} \end{bmatrix} = \begin{bmatrix} \cos\theta & -d\sin\theta \\ \sin\theta & d\cos\theta \\ 0 & 1 \end{bmatrix} \begin{bmatrix} v \\ \omega \end{bmatrix} \tag{1}$$

$$\overline{\boldsymbol{M}}(q)\dot{\boldsymbol{V}} + \overline{\boldsymbol{C}}(q,\dot{q})\boldsymbol{V} + \overline{\boldsymbol{F}} + \overline{\boldsymbol{\tau}}_d = \overline{\boldsymbol{B}}\boldsymbol{\tau} \tag{2}$$

where $\boldsymbol{q} = (x, y, \theta)^{\mathrm{T}}$ denotes the actual Cartesian position and orientation of the physical robot, (x, y) is the midpoint coordinate of the robot's wheel axle in the Cartesian coordinate system, θ is the orientation. $\boldsymbol{V} = [v \quad \omega]^{\mathrm{T}}$, v and ω represent the linear velocity and the angular velocity, respectively. $\overline{\boldsymbol{M}}(q) = \begin{bmatrix} m & 0 \\ 0 & I - md^2 \end{bmatrix}$ is the system inertial matrix, m and I represent the mass of the robot platform and the moment of inertia around the axle, respectively. d is the distance from the midpoint of the robot's wheel axle to the front of the robot. $\overline{\boldsymbol{C}}(q,\dot{q}) = \begin{bmatrix} 0 & 0 \\ 0 & 0 \end{bmatrix}$ is the centripetal and Coriolis matrix, $\overline{\boldsymbol{B}} = \dfrac{1}{r}\begin{bmatrix} 1 & 1 \\ R & -R \end{bmatrix}$, $2R$ is the distance between the driving wheels and r is the radius of the robot's wheels. $\overline{\boldsymbol{F}}$ is the friction, $\overline{\boldsymbol{\tau}}_d$ represents unknown bounded disturbances. $\boldsymbol{\tau} = [\tau_r \quad \tau_l]^{\mathrm{T}}$ is the input vector, τ_r and τ_l represent the driving torque applied to the right wheel and left wheel, respectively.

2.2 Kinematic model of the leader-follower formation

Consider the leader-follower robot system, which consists of two nonholonomic constrained robots with a relative distance of l_{ij} and a relative orientation of ψ_{ij}, shown in Fig. 1. The kinematics of the formation system are shown as follows [22]:

$$\begin{aligned} \dot{l}_{ij} &= v_j\cos\gamma_j - v_i\cos\psi_{ij} + d\omega_j\sin\gamma_j \\ \dot{\psi}_{ij} &= (v_i\sin\psi_{ij} - v_j\sin\gamma_j + d\omega_j\cos\gamma_j - l_{ij}\omega_i)/l_{ij} \end{aligned} \tag{3}$$

where $\gamma_j = \psi_{ij} + \theta_{ij}$, $\theta_{ij} = \theta_i - \theta_j$.

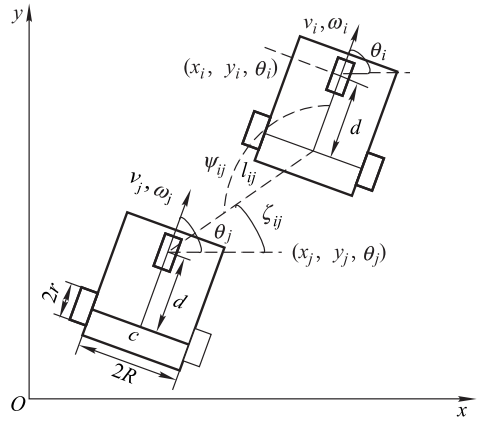

Fig. 1 Leader-follower robot system

Remark 1 In this paper, subscripts i and j of robot variables represent the parameters of the leader and the follower, respectively. If $j = 2$, that represents the second follower.

The kinematics state space equations of the leader-follower formation can be obtained by (3) as [22].

$$[\dot{l}_{ij} \quad \dot{\psi}_{ij}]^{\mathrm{T}} = \boldsymbol{f} + \boldsymbol{G}\boldsymbol{V}_j \tag{4}$$

where $\boldsymbol{G} = \begin{bmatrix} \cos\gamma_j & d\sin\gamma_j \\ -\dfrac{\sin\gamma_j}{l_{ij}} & \dfrac{d\cos\gamma_j}{l_{ij}} \end{bmatrix}$, $\boldsymbol{f} = \begin{bmatrix} -v_i\cos\psi_{ij} & \dfrac{v_i\sin\psi_{ij} - l_{ij}\omega_i}{l_{ij}} \end{bmatrix}^{\mathrm{T}}$.

3. Controller design

The design of the controller is carried out step by step. Firstly, the multivariable fixed-time formation controller is designed to realize formation tracking. Then, to achieve velocity tracking, the fixed-time dynamic torque controller is designed to overcome the uncertainty according to the robot dynamics model.

3.1 Fixed-time formation control

The relative lemmas and definitions are given before the design of the formation controller.

Definition 1 [18,23] Consider the following system

$$\begin{cases} \dot{\boldsymbol{x}} = g(t,x) \\ \boldsymbol{x}(0) = \boldsymbol{x}_0 \end{cases} \tag{5}$$

where $\boldsymbol{x} \in \mathbf{R}^n$ is the state vector, $g \in \mathbf{R}^+ \times \mathbf{R}^n \to \mathbf{R}^n$ is a locally measurable nonlinear function that is discontinuous with respect to the state variable $\boldsymbol{x}$. The origin of system (5) is fixed-time stable if it is globally finite-time stable and the settling-time function $T(\boldsymbol{x}_0)$ is bounded, i.e., $\exists T_{\max} > 0, T(x_0) \leqslant T_{\max}, \forall \boldsymbol{x}_0 \in \mathbf{R}^n$.

Lemma 1 [23] If there exists a continuous radially unbounded function $V(\boldsymbol{x}) : \mathbf{R}^n \to \mathbf{R}^+ \cup \{0\}$ with $V(\boldsymbol{x}) = 0 \Rightarrow \boldsymbol{x} = 0$ and any solution of (5) satisfies the inequality

$$\dot{V}(x(t)) \leqslant -\alpha V^P(x(t)) - \beta V^q(x(t)) \tag{6}$$

where $\alpha, \beta > 0$ and $p > 1 > q > 0$, the origin is globally fixed-time stable and the settling time function T is uniformly bounded by a computable constant, i.e.,

$$T \leqslant T_{\max} := \frac{1}{\alpha(p-1)} + \frac{1}{\beta(1-q)}. \tag{7}$$

Lemma 2 [23] Consider the first-order multivariable system

$$\dot{\boldsymbol{x}} = -\alpha \boldsymbol{x} \|\boldsymbol{x}\|^{p-1} - \beta \boldsymbol{x} \|\boldsymbol{x}\|^{q-1} \tag{8}$$

where $\boldsymbol{x} \in \mathbf{R}^n$, $\alpha, \beta > 0$ and $p > 1 > q > 0$. The system in (8) is globally fixed-time stable at the origin, in which the settling time estimate is given by (7).

The goal of the fixed-time formation control based on the leader-follower model is to find a velocity control input to satisfy that

$$\begin{cases} \lim\limits_{t \to T} (l_{ijd} - l_{ij}) = 0 \\ \lim\limits_{t \to T} (\psi_{ijd} - \psi_{ij}) = 0 \end{cases} \tag{9}$$

where l_{ijd} and ψ_{ijd} are the desired distance and relative orientation between the follower robot and the leader robot, respectively. The time T is independent of initial conditions and is only related to the design parameters of the designed controller. We mainly focus on the follower robot and make the following assumptions.

Assumption 1 The leader robot tracks a predefined time-varying trajectory.

Assumption 2 All states of the follower robot and the velocities of the leader robot are known by the follower robot.

3.2 Fixed-time kinematics formation controller based on the leader-follower model

For formation kinematics system (4), define control input as $\boldsymbol{V}_j = [v_j \quad \omega_j]^{\mathrm{T}}$. Since $\det G = d/l_{ij} \neq 0$, the matrix $\boldsymbol{G}$ is always invertible, we assume that desired values l_{ijd} and ψ_{ijd} are time invariant. Using the state feedback linearization, we design the fixed-time formation kinematics controller as follows:

$$\boldsymbol{V}_{jc} = \boldsymbol{G}^{-1}(-\boldsymbol{f} + \alpha_0 \boldsymbol{e}_j \|\boldsymbol{e}_j\|^{p_0 - 1} + \beta_0 \boldsymbol{e}_j \|\boldsymbol{e}_j\|^{q_0 - 1}) \tag{10}$$

where $\boldsymbol{e}_j = [e_{j1} \quad e_{j2}]^{\mathrm{T}} = [l_{ijd} - l_{ij} \quad \psi_{ijd} - \psi_{ij}]^{\mathrm{T}}$ is the formation tracking error and α_0, β_0, p_0, q_0 are design constants, satisfying $\alpha_0 > 0$, $\beta_0 > 0$, $p_0 > 1$, $0 < q_0 < 1$. Substituting the formation controller (10) and the formation kinematics system (4) into the derivative of the formation tracking error, the differential equation for formation tracking error can be obtained as follows:

$$\dot{\boldsymbol{e}}_j = -\alpha_0 \boldsymbol{e}_j \|\boldsymbol{e}_j\|^{p_0 - 1} - \beta_0 \boldsymbol{e}_j \|\boldsymbol{e}_j\|^{q_0 - 1}. \tag{11}$$

Theorem 1 Considering multivariable first-order systems (4) with the proposed fixed-time formation kinematics controller (10), the formation tracking error $\boldsymbol{e}_j$ will converge to the origin within a fixed time T_0, i.e., the follower implements formation tracking within setting time T_0 that is independent of the system state through the parameter design of the controller.

$$T_0 \leqslant T_{0\max} := \frac{1}{\alpha_0(p_0 - 1)} + \frac{1}{\beta_0(q_0 - 1)} \tag{12}$$

Proof Consider the following Lyapunov function:

$$L_0 = \frac{1}{2} \boldsymbol{e}_j^{\mathrm{T}} \boldsymbol{e}_j. \tag{13}$$

Take the derivative for (13) and substitute (11) into $\dot{L}_0$, we can obtain

$$\begin{aligned} \dot{L}_0 = &-\alpha_0 \boldsymbol{e}_j^{\mathrm{T}} \boldsymbol{e}_j \|\boldsymbol{e}_j\|^{p_0 - 1} - \beta_0 \boldsymbol{e}_j^{\mathrm{T}} \boldsymbol{e}_j \|\boldsymbol{e}_j\|^{q_0 - 1} = \\ &-\alpha_0 \|\boldsymbol{e}_j\|^{p_0 + 1} - \beta_0 \|\boldsymbol{e}_j\|^{q_0 + 1} = \\ &-\alpha_0 (2L_0)^{\frac{p_0 + 1}{2}} - \beta_0 (2L_0)^{\frac{q_0 + 1}{2}}. \end{aligned} \tag{14}$$

Let $y_0 = \sqrt{2L_0} \geqslant 0$, and we have $\dot{y}_0 = \dot{L}_0 / \sqrt{2L_0}$. It follows from (14) that $\dot{y}_0 = -\alpha_0 y_0^{p_0} - \beta_0 y_0^{q_0}$. Thus, by Lemma 1, the formation tracking partial differential equation (11) is globally fixed-time stable at the origin and the settling time is bounded by (12), i.e., l_{ij} and ψ_{ij} in system (4) reach l_{ijd} and ψ_{ijd} within a fixed time, which achieves the desired formation. According to Lemma 2, we can also get the above conclusion. □

3.3 Multivariate fixed-time dynamics torque controller based on observer

Adopting the designed speed controller (10) as the input, the fixed-time formation control problem at the level of formation kinematics is addressed, and it achieves the specified formation within a fixed time. However, in practical applications, robots are often affected by external disturbance, ground friction, and load change. It is necessary to design a fixed-time dynamics torque controller to overcome multiple uncertainties mentioned above.

The dynamics model (2) of the follower robot with multiple uncertainties can be expressed as

$$\dot{\boldsymbol{V}}_j = E_{0j}\boldsymbol{\tau}_j - \boldsymbol{H} \tag{15}$$

where $\boldsymbol{H}$ represents the total uncertainty, $\boldsymbol{H} = \overline{\boldsymbol{M}}_0^{-1}(\Delta\overline{\boldsymbol{M}}\dot{\boldsymbol{V}}_j + \Delta\boldsymbol{C}\boldsymbol{V}_j + \overline{\boldsymbol{F}} + \overline{\boldsymbol{\tau}}_d)$, $\Delta\overline{\boldsymbol{M}}$ and $\Delta\boldsymbol{C}$ are the uncertain parts of the inertia matrix and the Coriolis matrix respectively, $\boldsymbol{E}_{0j} = \overline{\boldsymbol{M}}^{-1}\overline{\boldsymbol{B}}$.

Assumption 3 The uncertainty of the follower robot is equivalent to the total bounded disturbance $\boldsymbol{H}$, and its derivative exists and is bounded, i.e., $\|\boldsymbol{H}\| \leqslant \delta$, δ is a positive constant, $\|\dot{\boldsymbol{H}}\| \leqslant h$, h is a positive constant.

The velocity (10) obtained by the formation controller is used as the desired velocity input of the dynamics (15) to design the fixed-time dynamics torque controller. Define the velocity tracking error as

$$\boldsymbol{e}_{jc} = \begin{bmatrix} e_{jc1} \\ e_{jc2} \end{bmatrix} = \boldsymbol{V}_{jc} - \boldsymbol{V}_j = \begin{bmatrix} v_{jc} - v_j \\ \omega_{jc} - \omega_j \end{bmatrix}. \tag{16}$$

Differentiating (16) and substituting (15), the velocity tracking error dynamics is yielded as

$$\dot{\boldsymbol{e}}_{jc} = -E_{0j}\boldsymbol{\tau}_j + \boldsymbol{H} + \dot{\boldsymbol{V}}_{jc}. \tag{17}$$

Using the state feedback technology, we design a fixed-time dynamics torque controller as

$$\boldsymbol{\tau}_j = \boldsymbol{E}_{0j}^{-1}(\dot{\boldsymbol{V}}_{jc} + \alpha_1\boldsymbol{e}_{jc}\|\boldsymbol{e}_{jc}\|^{p_1-1} + \beta_1\boldsymbol{e}_{jc}\|\boldsymbol{e}_{jc}\|^{q_1-1} + \boldsymbol{H}) \tag{18}$$

where α_1, β_1, p_1 and q_1 are design constants, satisfying $\alpha_1 > 0, \beta_1 > 0, p_1 > 1, 0 < q_1 < 1$.

In fact, in the case of the structural and non-structural uncertainties such as load change, friction, and external disturbance, the uncertain part is difficult to obtain accurately even on its upper bound. Using the robust switch control is easy to cause the chattering problem in control input. A fixed-time observer is designed based on [20] and used to estimate the system uncertainty disturbance $\boldsymbol{H}$. The uncertain disturbance observer corresponding to (17) is designed as follows:

$$\begin{cases} \dot{\widehat{\boldsymbol{e}}}_{jc} = \dot{V}_{jc} + \widehat{\boldsymbol{H}} - E_{0j}\boldsymbol{\tau}_j - \\ \qquad k_1\boldsymbol{e}_1\|\boldsymbol{e}_1\|^{a_1-1} - \kappa_1\boldsymbol{e}_1\|\boldsymbol{e}_1\|^{b_1-1} \\ \dot{\widehat{\boldsymbol{H}}} = -k_2\boldsymbol{e}_1\|\boldsymbol{e}_1\|^{a_2-1} - \kappa_2\boldsymbol{e}_1\|\boldsymbol{e}_1\|^{b_2-1} \end{cases} \tag{19}$$

where $\widehat{\boldsymbol{e}}_{jc}$ and $\widehat{\boldsymbol{H}}$ are the estimates of $\boldsymbol{e}_{jc}$ and $\boldsymbol{H}$, respectively. k_1, k_2, κ_1 and κ_2 are observer gains. $a_1 \in (1-\varepsilon, 1)$, ε is a sufficiently small number, $a_2 = 2a_1 - 1$. Similarly, $b_1 \in (1, 1+\varepsilon_1)$, $b_2 = 2b_1 - 1$, ε_1 is a sufficiently small number. Defining $\boldsymbol{e}_1 = \widehat{\boldsymbol{e}}_{jc} - \boldsymbol{e}_{jc}$ and $\boldsymbol{e}_2 = [e_{21} \quad e_{22}]^{\mathrm{T}} = \widehat{\boldsymbol{H}} - \boldsymbol{H}$, the observer estimation error system is yielded as

$$\begin{cases} \dot{\boldsymbol{e}}_1 = \boldsymbol{e}_2 - k_1\boldsymbol{e}_1\|\boldsymbol{e}_1\|^{a_1-1} - \kappa_1\boldsymbol{e}_1\|\boldsymbol{e}_1\|^{b_1-1} \\ \dot{\boldsymbol{e}}_2 = -k_2\boldsymbol{e}_1\|\boldsymbol{e}_1\|^{a_2-1} - \kappa_2\boldsymbol{e}_1\|\boldsymbol{e}_1\|^{b_2-1} - \dot{\boldsymbol{H}} \end{cases}. \tag{20}$$

Theorem 2 Considering the observer (19) and the corresponding estimation error system (20), if Assumption 3 holds, then the errors $\boldsymbol{e}_1$ and $\boldsymbol{e}_2$ converge to the origin and the observer states $\widehat{\boldsymbol{e}}_{jc}$ and $\widehat{\boldsymbol{H}}$ converge to the state variables $\boldsymbol{e}_{jc}$ and $\boldsymbol{H}$, respectively, within a fixed-time T_g.

$$T_g \leqslant \frac{\lambda_{\max}^{\rho_1}(\boldsymbol{P}_1)}{r_1\rho_1} + \frac{1}{r_2\sigma\gamma^{\sigma}} \tag{21}$$

where $\rho_1 = 1 - a_1$, $\sigma = b_1 - 1$, $r_c = \dfrac{\lambda_{\min}(\boldsymbol{Q}_c)}{\lambda_{\max}(\boldsymbol{P}_c)}$, $c = 1, 2$, $\lambda_{\max}(\boldsymbol{P}_c)$ is the maximum eigenvalue of the matrix $\boldsymbol{P}_c$, $\lambda_{\max}(\boldsymbol{Q}_c)$ is the minimum eigenvalue of the matrix $\boldsymbol{Q}_c$, both $\lambda_{\max}(\boldsymbol{P}_c)$ and $\lambda_{\max}(\boldsymbol{Q}_c)$ are positive. $\boldsymbol{Q}_c$ is a positive definite matrix and the matrix $\boldsymbol{P}_c$ satisfies

$$\begin{cases} \boldsymbol{P}_1\boldsymbol{A}_1 + \boldsymbol{A}_1^{\mathrm{T}}\boldsymbol{P}_1 = -\boldsymbol{Q}_1 \\ \boldsymbol{P}_2\boldsymbol{A}_2 + \boldsymbol{A}_2^{\mathrm{T}}\boldsymbol{P}_2 = -\boldsymbol{Q}_2 \end{cases} \tag{22}$$

where $\boldsymbol{A}_1$ and $\boldsymbol{A}_2$ are defined as

$$\begin{cases} \boldsymbol{A}_1 = \begin{bmatrix} -k_1 & 1 \\ -k_2 & 0 \end{bmatrix} \\ \boldsymbol{A}_2 = \begin{bmatrix} -\kappa_1 & 1 \\ -\kappa_2 & 0 \end{bmatrix}. \end{cases} \tag{23}$$

Theorem 2 was proved in [20].

Then the new torque controller can be designed as

$$\boldsymbol{\tau}_j = \boldsymbol{E}_{0j}^{-1}(\dot{\boldsymbol{V}}_{jc} + \alpha_1\boldsymbol{e}_{jc}\|\boldsymbol{e}_{jc}\|^{p_1-1} + \beta_1\boldsymbol{e}_{jc}\|\boldsymbol{e}_{jc}\|^{q_1-1} + \widehat{\boldsymbol{H}}). \tag{24}$$

Substituting (24) into (17) yields

$$\dot{\boldsymbol{e}}_{jc} = -\alpha_1\boldsymbol{e}_{jc}\|\boldsymbol{e}_{jc}\|^{p_1-1} - \beta_1\boldsymbol{e}_{jc}\|\boldsymbol{e}_{jc}\|^{q_1-1} + \boldsymbol{H} - \widehat{\boldsymbol{H}}. \tag{25}$$

Theorem 3 Considering the velocity tracking system (17), if Assumption 3 holds, then, applying the torque controller (24) and the fixed-time observer (19), the system velocity tracking error $\boldsymbol{e}_{jc}$ will converge to the origin within a fixed time $T_g + T_1$. The upper bound of the convergence time T_1 can be obtained as

$$T_1 \leqslant T_{1\max} := \frac{1}{\alpha_1(p_1 - 1)} + \frac{1}{\beta_1(q_1 - 1)}. \tag{26}$$

Proof Consider the following Lyapunov function

$$L_1 = \frac{1}{2}\boldsymbol{e}_{jc}^{\mathrm{T}}\boldsymbol{e}_{jc}. \tag{27}$$

Taking the derivative of L_1 and substitution of (25) yields

$$\dot{L}_1 = \boldsymbol{e}_{jc}^{\mathrm{T}}\dot{\boldsymbol{e}}_{jc} = \boldsymbol{e}_{jc}^{\mathrm{T}}(-\alpha_1\boldsymbol{e}_{jc}\|\boldsymbol{e}_{jc}\|^{p_1-1} - \beta_1\boldsymbol{e}_{jc}\|\boldsymbol{e}_{jc}\|^{q_1-1} + \boldsymbol{H} - \widehat{\boldsymbol{H}}). \tag{28}$$

With the proposed fixed-time disturbance observer for uncertainties and Theorem 2, we realize the uncertainty estimation within a fixed time T_g, i.e., $\widehat{H} = H$. Equation (28) can be written as

$$\dot{L}_1 = -\alpha_1 \|\boldsymbol{e}_{jc}\|^{p_1+1} - \beta_1 \|\boldsymbol{e}_{jc}\|^{q_1+1} = -\alpha_1 (2L_1)^{\frac{p_1+1}{2}} - \beta_1 (2L_1)^{\frac{q_1+1}{2}}. \quad (29)$$

The proof of Theorem 1 shows that this system can realize velocity tracking in a fixed time $T_g + T_1$. □

Remark 3 The desired formation based on the fixed-time observer to estimate the uncertainty part is achieved within $T_{0\max}$. The followers affected by the uncertainty factors such as load change, friction, and external disturbance achieve velocity tracking within $T_g + T_{1\max}$. Taking $T = \max(T_{0\max}, T_g + T_{1\max})$, by designing control parameters, the desired formation can be achieved within T under the influence of multiple uncertainties.

4. Simulation and results analysis

In this paper, assisted by MATLAB/Simulink, the observer-based multivariable fixed-time formation control algorithm (OMFTFC) of mobile robots is simulated and analyzed. The algorithm is composed of the multivariable fixed-time formation controller and multivariable fixed-time dynamic moment controller based on the observer. The physical parameters of formation robots with uncertainties of load change, friction and disturbance are the same, as shown in Table 1.

Table 1 Physical parameters of the robot system model

Parameter	Value
R/m	0.153
r/m	0.03
d/m	0.25
m/kg	4, $t < 6$ s 5, $t \geqslant 6$ s
I/kg·m^2	2.5, $t < 6$ s 3, $t \geqslant 6$ s
$\overline{\boldsymbol{\tau}}_d$	$[0.1\sin(t-8) \quad 0.1\sin(t-8)]^{\mathrm{T}}$
$\overline{\boldsymbol{F}}$	$[0.25\mathrm{sign}(v) + 0.1v \quad 0.15\mathrm{sign}(\omega) + 0.3\omega]^{\mathrm{T}}$

To demonstrate the effectiveness of the proposed algorithm, the following three kinds of simulation are carried out. In the first case, a triangular formation ($l_{ijd} = 1, \psi_{ijd} = \pm 120°$) of three nonholonomic mobile robots is used as the research object to track the circular trajectory. The trajectory parameters are listed as follows: $v_r = 2$ m/s, $\omega_r = 0.4$ rad/s. Take the same observer parameters, $k_1 = k_2 = \kappa_1 = \kappa_2 = 2$, $a_1 = 0.6$, $b_1 = 1.8$. Take the same controller parameters, $\alpha_0 = \beta_0 = 1$, $p_0 = 2$, $q_0 = q_1 = 0.5$, $\alpha_1 = \beta_1 = 2$, $p_1 = 2$, and different formation initial position errors: (a) $[1.5 \quad \pi/6 \quad 2 \quad -\pi/6]$, (b) $[0.5 \quad -\pi/6 \quad 0.5 \quad \pi/6]$, (c) $[0.5 \quad \pi/4 \quad 0.5 \quad -\pi/4]$. The simulation results are shown in Figs. 2–6, where subfigures represent the simulation of the initial position error of (a), (b), and (c), respectively.

Fig. 2 demonstrates that the OMFTFC algorithm achieves a good tracking of the circular trajectory within a fixed time and overcomes the influence of uncertainty factors. Fig. 3 and Fig. 4 show the behaviour of the tracking error, which demonstrates that the follower robots with different initial states reach the desired formation position within the fixed design time, and indicates that the convergence time of the proposed fixed-time algorithm is independent of the initial state of robots.

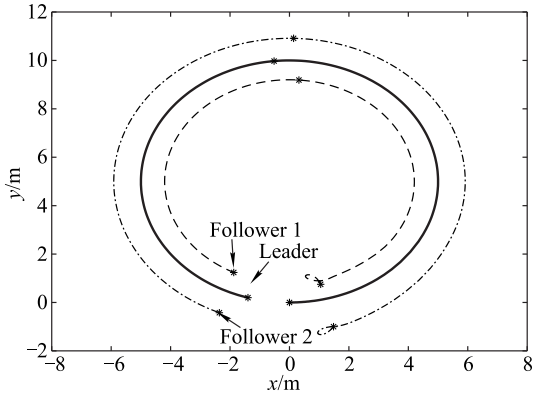

(a) Initial position error [1.5 π/6 2 −π/6]

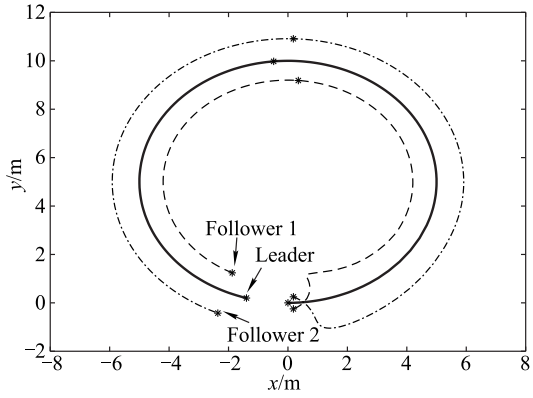

(b) Initial position error [0.5 π/6 0.5 −π/6]

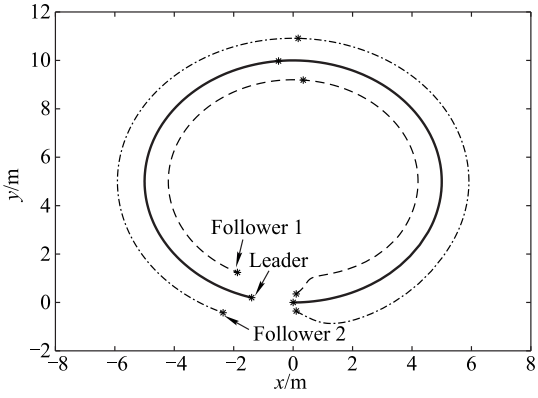

(c) Initial position error [0.5 π/4 0.5 −π/4]

Fig. 2 Triangular formation tracking circular trajectory

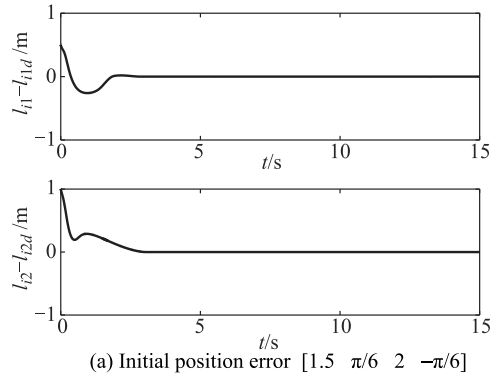

(a) Initial position error [1.5 π/6 2 −π/6]

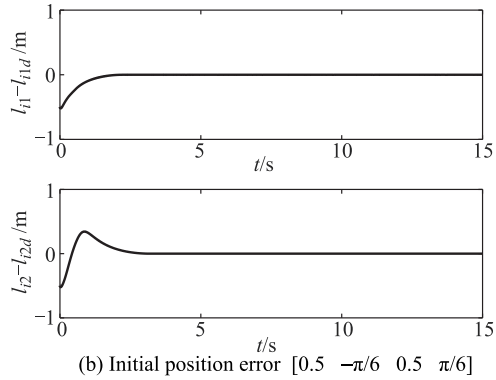

(b) Initial position error [0.5 −π/6 0.5 π/6]

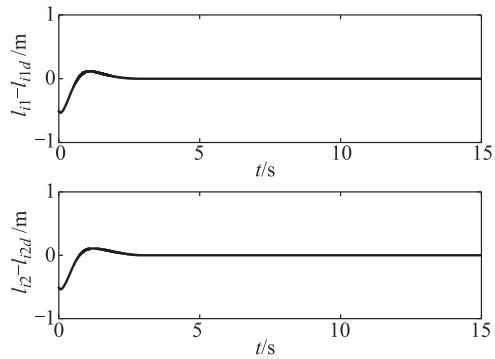

(c) Initial position error [0.5 π/4 0.5 −π/4]

Fig. 3 Tracking errors of relative distance from follower to leader (triangular formation)

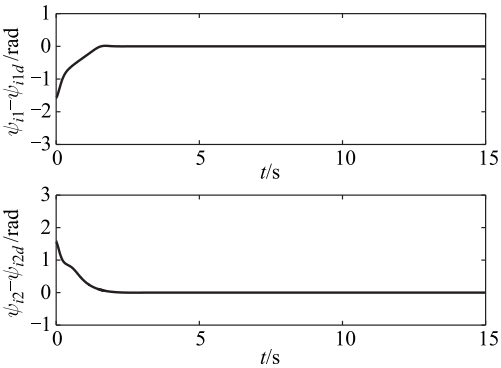

(a) Initial position error [1.5 π/6 2 −π/6]

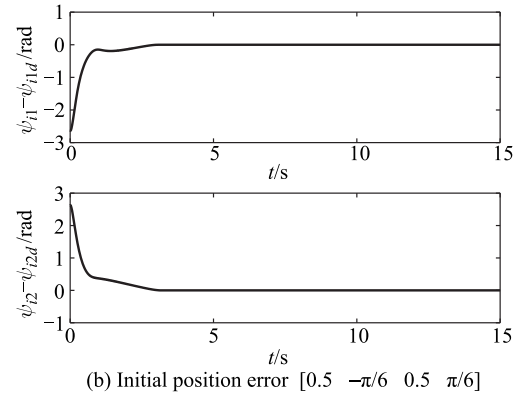

(b) Initial position error [0.5 −π/6 0.5 π/6]

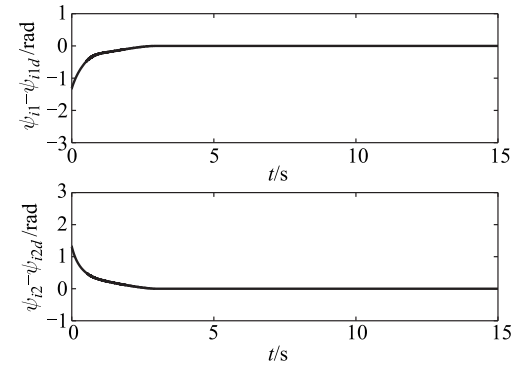

(c) Initial position error [0.5 π/4 0.5 −π/4]

Fig. 4 Tracking errors of relative orientation from follower to leader (triangular formation)

Fig. 5 and Fig. 6 show that followers achieve the track reference velocity within a fixed time, indicating that the OMFTFC algorithm has better performance.

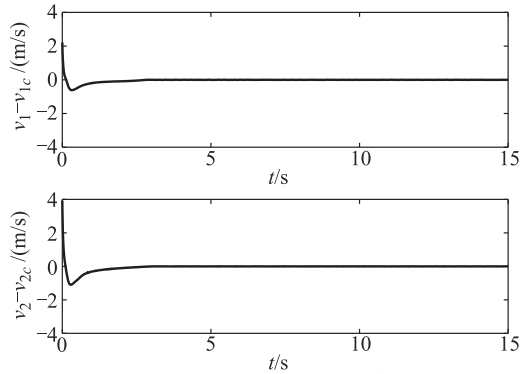

(a) Initial position error [1.5 π/6 2 −π/6]

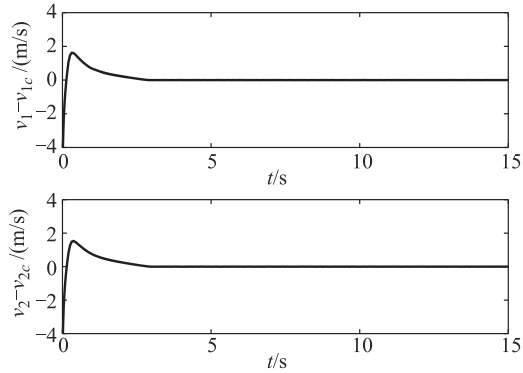

(b) Initial position error [0.5 −π/6 0.5 π/6]

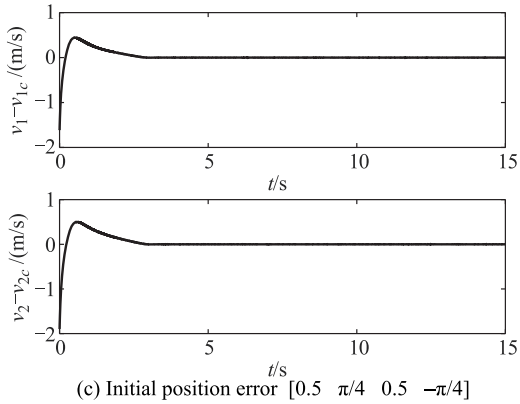

(c) Initial position error [0.5 π/4 0.5 −π/4]

Fig. 5 Velocity tracking errors of followers (triangular formation)

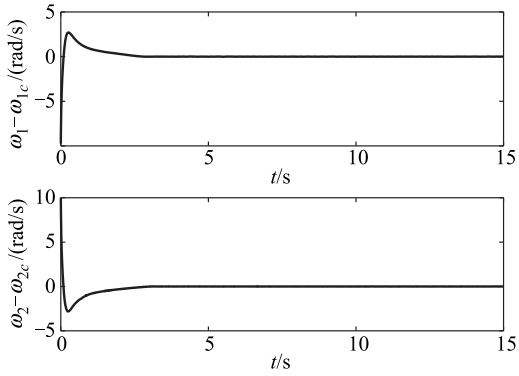

(a) Initial position error [1.5 π/6 2 −π/6]

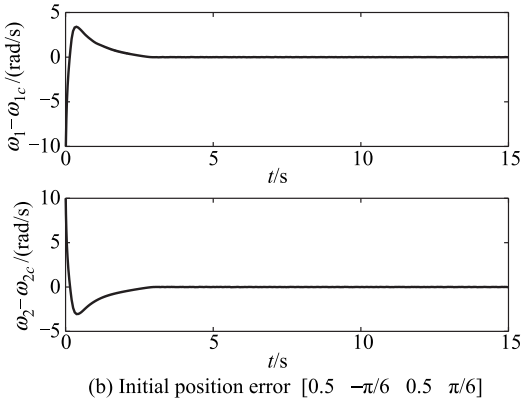

(b) Initial position error [0.5 −π/6 0.5 π/6]

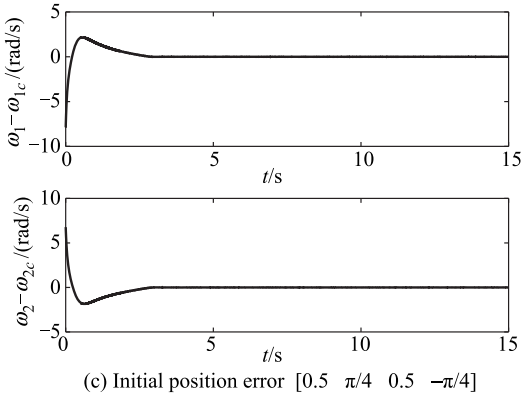

(c) Initial position error [0.5 π/4 0.5 −π/4]

Fig. 6 Angular velocity tracking errors of followers (triangular formation)

We carry out the second simulation in order to compare with the multivariable finite-time formation control based on observer (MFTFCO). Based on [20], the finite-time formation controller and the finite-time observer used in the simulation are shown in (30) – (32).

$$\boldsymbol{V}_{jc} = \boldsymbol{G}^{-1}(-\boldsymbol{f} + \alpha_0 \boldsymbol{e}_j \|\boldsymbol{e}_j\|^{p_0-1}) \tag{30}$$

$$\boldsymbol{\tau}_j = \boldsymbol{E}_{0j}^{-1}(\dot{\boldsymbol{V}}_{jc} + \alpha_1 \boldsymbol{e}_{jc} \|\boldsymbol{e}_{jc}\|^{p_1-1} + \widehat{\boldsymbol{H}}) \tag{31}$$

$$\begin{cases} \dot{\widehat{\boldsymbol{e}}}_{jc} = \dot{V}_{jc} + \widehat{\boldsymbol{H}} - E_{0j}\boldsymbol{\tau}_j - k_1 \boldsymbol{e}_1 \|\boldsymbol{e}_1\|^{a_1-1} \\ \widehat{\boldsymbol{H}} = -k_2 \boldsymbol{e}_1 \|\boldsymbol{e}_1\|^{a_2-1} \end{cases} \tag{32}$$

We take the same object, trace trajectory, control parameters, observer parameters and three initial position differences as the first simulation. The simulation results are shown in Figs. 7 – 11, where subfigures represent the simulation of the initial position error of (a), (b), and (c), respectively.

From Figs. 7 – 11 and their comparison with Figs. 2 – 6, it can be seen that the OMFTFC algorithm proposed in this paper has a better convergence speed. The convergence time of the OMFTFC algorithm is independent of the initial state of the system and only determined by the control algorithm design parameters. However, the MFTFCO algorithm is greatly affected by the initial state of the system.

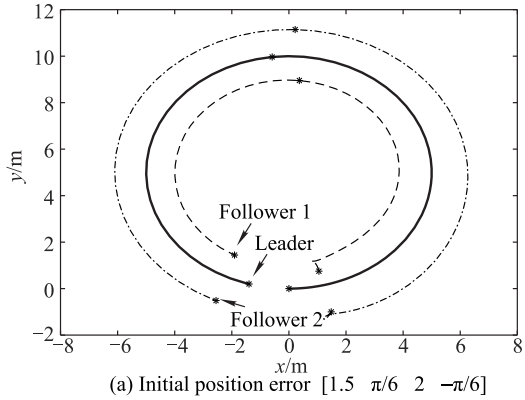

(a) Initial position error [1.5 π/6 2 −π/6]

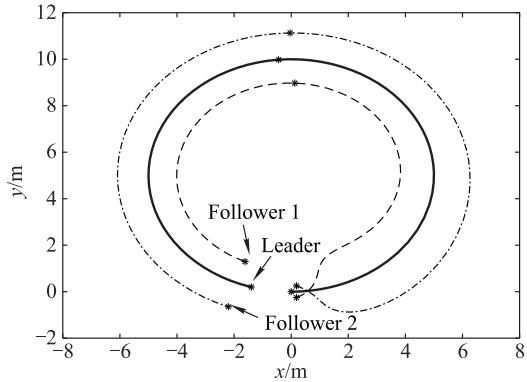

(b) Initial position error [0.5 −π/6 0.5 π/6]

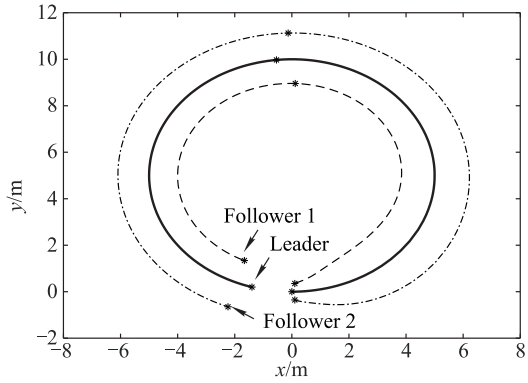

(c) Initial position error [0.5 π/4 0.5 −π/4]

Fig. 7 Triangular formation tracking circular trajectory based on MFTFCO

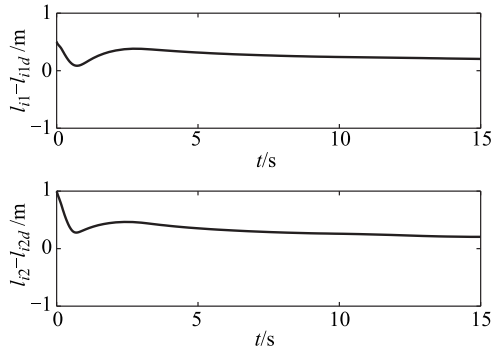

(a) Initial position error [1.5 π/6 2 −π/6]

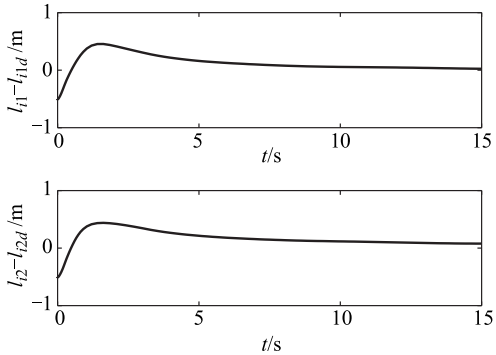

(b) Initial position error [0.5 −π/6 0.5 π/6]

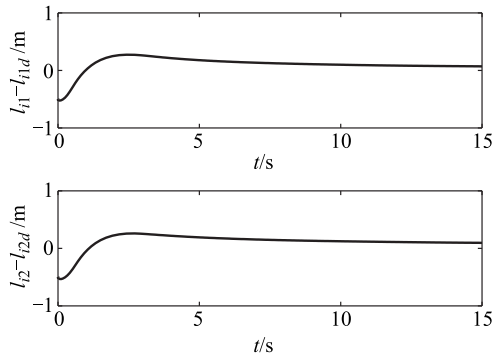

(c) Initial position error [0.5 π/4 0.5 −π/4]

Fig. 8 Tracking errors of relative distance from follower to leader (triangular formation) based on MFTFCO

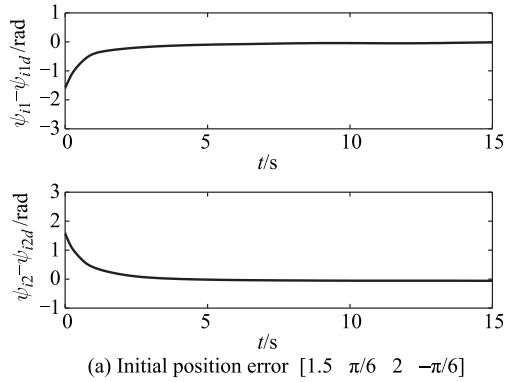

(a) Initial position error [1.5 π/6 2 −π/6]

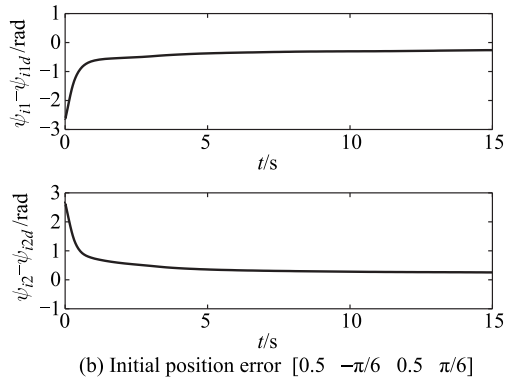

(b) Initial position error [0.5 −π/6 0.5 π/6]

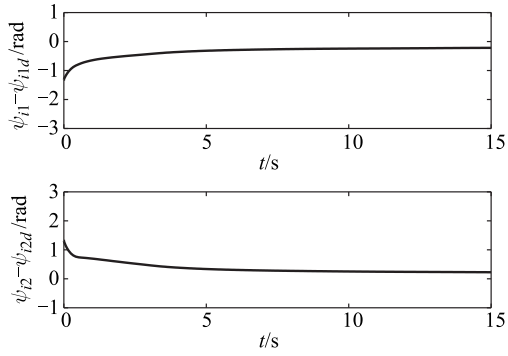

(c) Initial position error [0.5 π/4 0.5 −π/4]

Fig. 9 Tracking errors of relative orientation from follower to leader (triangular formation) based on MFTFCO

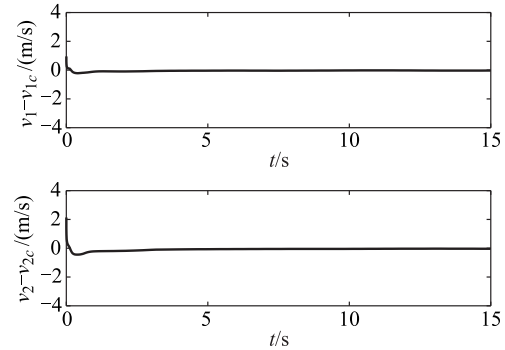

(a) Initial position error [1.5 π/6 2 −π/6]

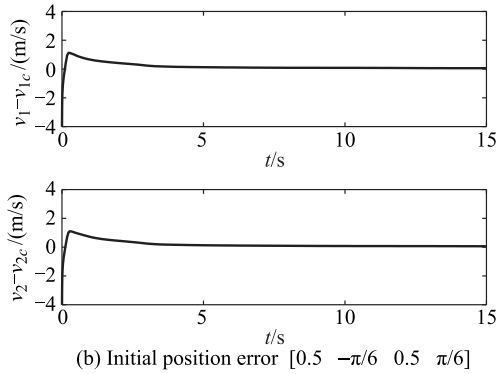

(b) Initial position error [0.5 −π/6 0.5 π/6]

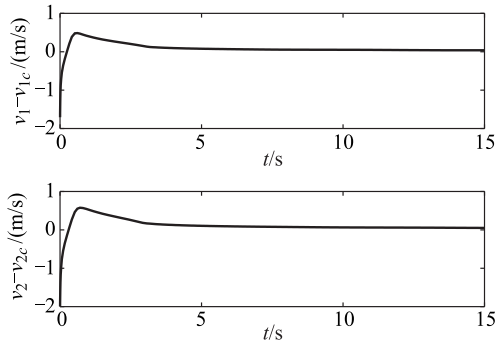

(c) Initial position error [0.5 π/4 0.5 −π/4]

Fig. 10 Velocity tracking errors of followers (triangular formation) based on MFTFCO

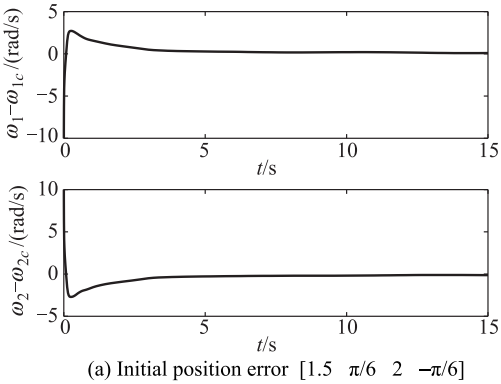

(a) Initial position error [1.5 π/6 2 −π/6]

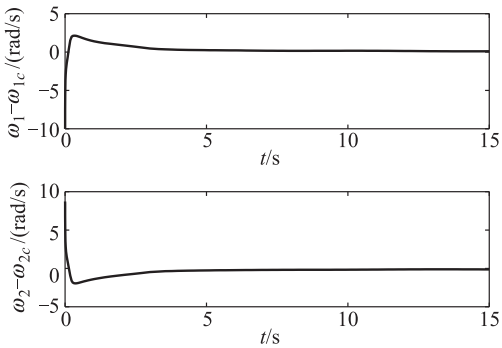

(b) Initial position error [0.5 −π/6 0.5 π/6]

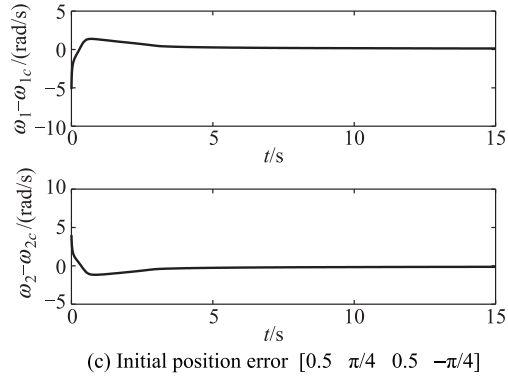

(c) Initial position error [0.5 π/4 0.5 −π/4]

Fig. 11 Angular velocity tracking errors of followers (triangular formation) based on MFTFCO

We carry out the third simulation in order to further verify the effectiveness of the OMFTFC algorithm. We mainly intent to verify that the fixed-time control is independent of the initial state by designing controller parameters, and the uncertainty part can be estimated by designing a fixed-time observer. In the third case, a formation consisting of two robots ($l_{i1d} = 1, \psi_{i1d} = 120°$) is employed as a research object to track the circular trajectory. The trajectory parameters are listed as follows: $v_r = 2$ m/s, $\omega_r = 0.4$ rad/s. The observer parameters are the same as the triangular formation in the first case. Take the same controller parameters: $\alpha_0 = \beta_0 = 1$, $p_0 = 2$, $\alpha_1 = 2$, $\beta_1 = 3$, $q_0 = q_1 = 0.5$, $p_1 = 2.5$. The simulation results are shown in Figs. 12 – 15, subfigures represent the simulation of three uncertainties (a), (b), and (c), respectively. (a) Formation initial position error is assigned as $[0.5 \quad \pi/3]$, the load change, friction and external disturbance of the robot are the same as in the triangle formation. (b) Formation initial position error is assigned as $[0.8 \quad \pi/4]$. Taking external disturbance as $[0.2\sin(t-6) \quad 0.2\sin(t-6)]^{\mathrm{T}}$, it can be seen that the magnitude of the disturbance and its time acting on the system are changed. (c) Formation initial position error is assigned as $[1.5 \quad \pi/3]$, on the basis of (b), the load change time is delayed by 2 s, i.e., $m = 5, t \geqslant 8$ s, $I = 3, t \geqslant 8$ s.

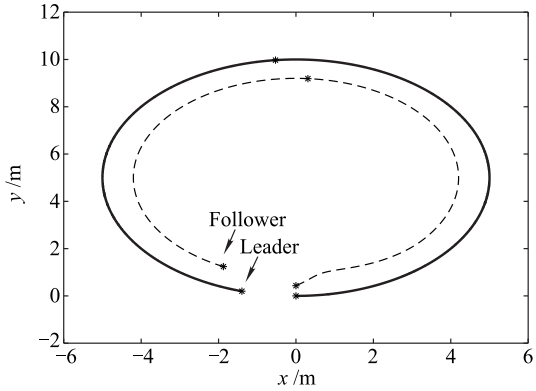

(a) Initial position error [0.5 π/3]

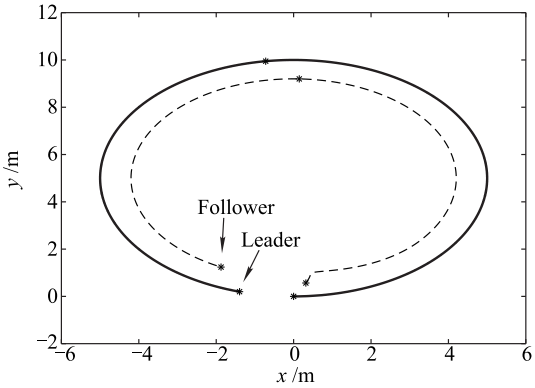

(b) Initial position error [0.8 π/4]

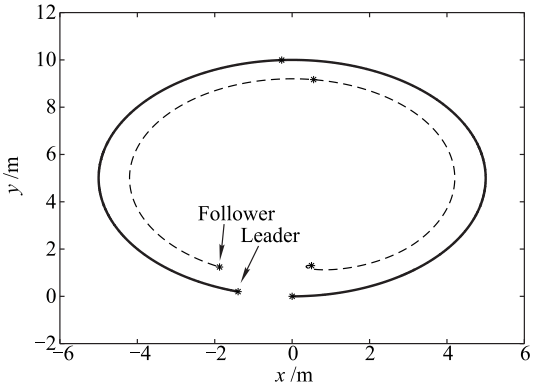

(c) Initial position error [0.5 π/3]

Fig. 12 Double robot formation tracking circular trajectory

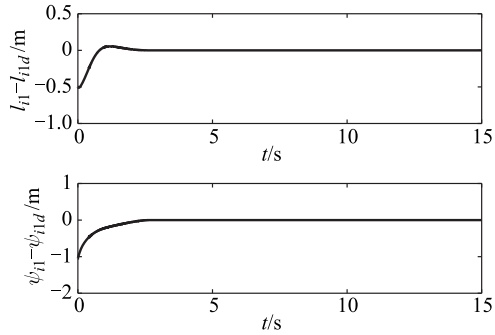

(a) Initial position error [0.5 π/3]

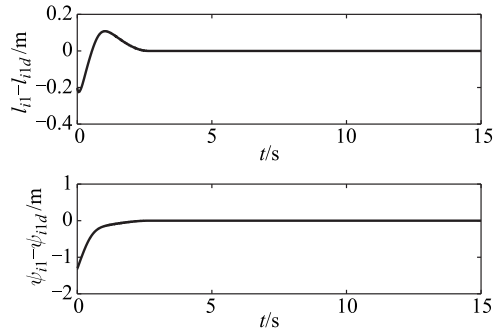

(b) Initial position error [0.8 π/4]

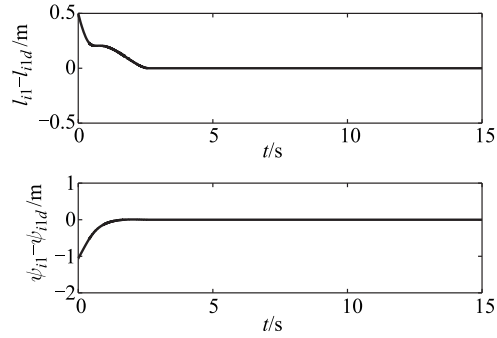

(c) Initial position error [1.5 π/3]

Fig. 13 Tracking errors of relative distance and relative orientation from the follower to the leader (double robot formation)

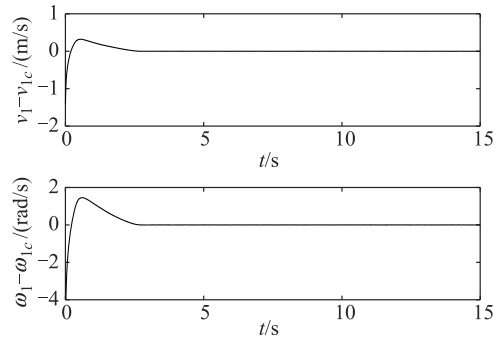

(a) Initial position error [0.5 π/3]

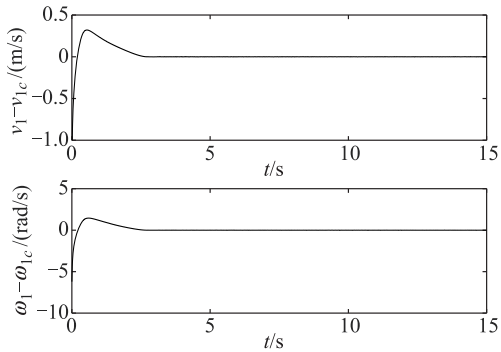

(b) Initial position error [0.8 π/4]

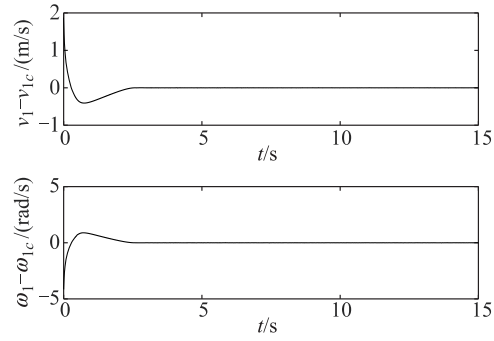

(c) Initial position error [1.5 π/3]

Fig. 14 Velocity and angular velocity tracking errors of the follower (double robot formation)

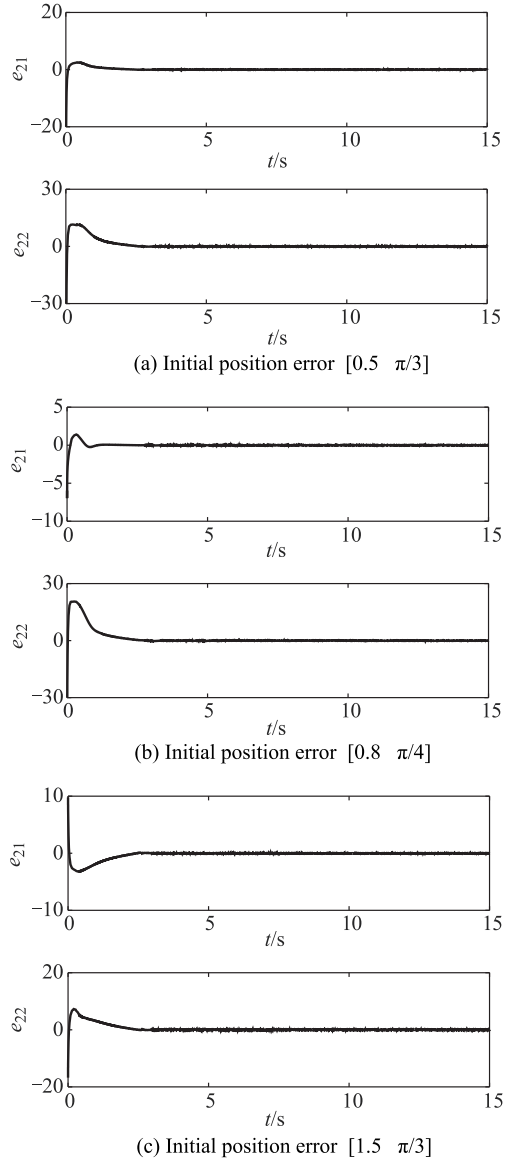

(a) Initial position error [0.5 π/3]

(b) Initial position error [0.8 π/4]

(c) Initial position error [1.5 π/3]

Fig. 15 Estimated error of the uncertain part of the follower (double robot formation)

In Figs. 12 – 15, $l_{i1} - l_{i1d}$ represents the relative distance error between the leader and the follower, $\psi_{i1} - \psi_{i1d}$ represents the relative orientation error between the leader and the follower, $v_1 - v_{1c}$ represents the velocity tracking error, $\omega_1 - \omega_{1c}$ represents the angular velocity tracking error, and e_{21} and e_{22} represent the estimated error of the uncertain part for the follower. All these parameters converge within a fixed time, which is independent of the initial position error and the magnitude of the uncertainty. From Figs. 12 – 15, it can be seen that the OMFTFC algorithm achieves better formation tracking in the designed time.

5. Conclusions

This paper proposes a multivariable fixed-time leader-follower formation control strategy for mobile robots based on the multivariable fixed-time disturbance observer in the framework of the multivariate fixed-time theory, which overcomes multiple uncertainties of the nonholonomic mobile robot system in real applications. The algorithm can realize the desired formation within the fixed time that is independent of the initial state through parameter design. Our method can overcome the drawbacks caused by the initial state in the finite-time observer, which makes the observation time easy to obtain. At the same time, it also provides a solution for other multivariable fixed-time control systems to overcome multiple uncertain. Based on the state space model of the leader-follower formation, a cascade multivariable fixed-time control structure for nonholonomic mobile robots is presented, which provides a new basic framework for the extended research of such problems. The experimental results demonstrate that our method can successfully increase the practicability of the formation robot system in which the formation has time-bound requirements in the presence of multiple uncertainties. Our method can be further extended to input-limited multivariate fixed-time formation control in future.

References

[1] DIERKS T, JAGANNATHAN S. Neural network control of mobile robot formations using RISE feedback. IEEE Trans. on Systems, Man, and Cybernetics-PART B: Cybernetics, 2009, 39(2): 332 – 347.

[2] DIERKS T, JAGANNATHAN S. Neural network output feedback control of robot formations. IEEE Trans. on Systems, Man, and Cybernetics-Part B: Cybernetics, 2010, 40(2): 383 – 398.

[3] PARK B S, PARK J B, CHOI Y H. Robust adaptive formation control and collision avoidance for electrically driven nonholonomic mobile robots. IET Control Theory and Applications, 2011, 5(3): 514 – 522.

[4] ZHU L, LI Y, SUN M, et al. Sliding mode control of mobile robot formations based on neural networks. Electric Machines and Control, 2014, 18(3): 527 – 538. (in Chinese)

[5] ZHAO D, ZOU T. A finite-time approach to formation control of multiple mobile robots with terminal sliding mode. International Journal of Systems Science, 2012, 43(11): 1998 – 2014.

[6] GHASEMI M, NERSESOV S G. Sliding mode cooperative control for multirobot systems: a finite-time approach. Mathematical Problems in Engineering, 2013: 1 – 16.

[7] OU M, DU H, LI S. Finite-time formation control of multiple nonholonomic mobile robots. International Journal of Robust and Nonlinear Control, 2014, 24(1): 140 – 165.

[8] DU H, WEN G, CHENG Y, et al. Distributed finite-time cooperative control of multiple high-order nonholonomic mobile robots. IEEE Trans. on Neural Networks and Learning Systems, 2017, 28(12): 2998 – 3006.

[9] DU H, WEN G, YU X, et al. Finite-time consensus of multiple nonholonomic chained-form systems based on recursive distributed observer. Automatica, 2015, 62: 236 – 242.

[10] CHENG Y, JIA R, DU H, et al. Robust finite-time consensus formation control for multiple nonholonomic wheeled mobile robots via output feedback. International Journal of Robust and Nonlinear Control, 2017, 28(6): 2082 – 2096.

[11] ZHANG C, SUN T, PAN Y. Neural network observer-based finite time formation control of mobile robots. Mathematical

Problems in Engineering, 2014: 1 – 9.
[12] POLYAKOV, A. Nonlinear feedback design for fixed-time stabilization of linear control systems. IEEE Trans. on Automatic Control, 2012, 57(8): 2106 – 2110.
[13] ZUO Z, TIE L. Distributed robust finite-time nonlinear consensus protocols for multi-agent systems. International Journal of Systems Science, 2016, 47(6): 1366 – 1375.
[14] CHU X, PENG Z, WEN G. Robust fixed-time consensus tracking with application to formation control of unicycles. IET Control Theory and Apolications, 2018, 12(1): 53 – 59.
[15] WANG C, TNUNAY H, ZUO Z, et al. Fixed-time formation control of multi-robot systems: design and experiments. IEEE Trans. on Industrial Electronics, 2019, 66(8): 6292 – 6301.
[16] ZUO Z. Nonsingular fixed-time consensus tracking for second-order multi-agent networks. Automatica, 2015, 54: 305 – 309.
[17] DEFOOT M, POLYAKOV A, DEMESURE G, et al. Leader-follower fixed-time consensus for multi-agent systems with unknown non-linear inherent dynamics. IET Control Theory and Applications, 2015, 9(14): 2165 – 2170.
[18] HONG H, YU W, WEN G, et al. Distributed robust fixed-time consensus for nonlinear and disturbed multiagent systems. IEEE Trans. on Systems, Man, and Cybernetics: Systems, 2017, 47(7): 1464 – 1473.
[19] ZUO Z, TIAN B, DEFOOT M, et al. Fixed-time consensus tracking for multiagent systems with high-order integrator dynamics. IEEE Trans. on Automatic Control, 2018, 63(2): 563 – 570.
[20] BASIN M, YU P, SHTESSEL Y. Finite- and fixed-time differentiators utilizing HOSM techniques. IET Control Theory and Applications, 2017, 11(8): 1144 – 1152.
[21] BASIN M, PABLO R R, ALISON G A. Continuous fixed-time convergent super-twisting algorithm in case of unknown state and disturbance initial conditions. Asian Journal of Control, 2019, 21(1): 1 – 16.
[22] SHEN D, SUN W, SUN Z. Adaptive PID formation control of nonholonomic robots without leader's velocity information. ISA Transactions, 2014, 53(2): 474 – 480.
[23] ZUO Z, DEFOOT M, TIAN B, et al. Fixed time stabilization of second-order uncertain multivariable nonlinear systems. Proc. of the 35th Chinese Control Conference, 2016: 907 – 912.

Biographies

LI Yandong was born in 1978. He received his B.S. degree in automation from Qiqihar University, Qiqihar, China, in 2001, M.S. degree in control theory and control engineering from Harbin Engineering University in 2008, and Ph.D. degree in detection technology and automatic equipment from Harbin Engineering University in 2011. He was a visiting scholar in Northeastern University, Liaoning, Shenyang, China, in 2018 and 2019. He is currently an associate professor in Qiqihar University. His research interests include robot control, neural networks, and formation control.
E-mail: liyandong1234@126.com

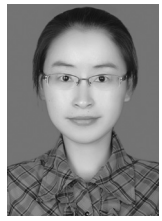

ZHU Ling was born in 1981. She received her B.S. degree in automation from Qiqihar University in 2004, M.S. degree in control theory and control engineering from Harbin Engineering University in 2009, and Ph.D. degree in pattern recognition and intelligent systems from Harbin Engineering University in 2012. She is currently a lecturer in Qiqihar University. Her research interests include robot control, virtual surgery, and intelligent control.
E-mail: zhuling_ruby2010@163.com

GUO Yuan was born in 1974. She received her B.S. degree in automation from Qiqihar University in 1997, and M.S. and Ph.D. degrees in electrical engineering from Yan Shan University, in 2004 and 2008, respectively. She was a visiting scholar in Johns Hopkings University, Baltimore, Maryland, U.S. in 2012 and 2013. She is currently a professor of computer science and technology in Qiqihar University. Her research interests include photo electric detection, optical image encryption, sensor technology, and image processing.
E-mail: guoyuan171@126.com